Protist, Vol. 170, 358–373, August 2019
http://www.elsevier.de/protis
Published online date 5 July 2019

Protist

ORIGINAL PAPER

Integrated Genomic and Transcriptomic Analysis of the Peridinin Dinoflagellate *Amphidinium carterae* Plastid

Richard G. Dorrell[1,2], R. Ellen R. Nisbet[1], Adrian C. Barbrook, Stephen J.L. Rowden, and Christopher J. Howe[3]

Department of Biochemistry, University of Cambridge, United Kingdom

Submitted March 7, 2019; Accepted June 14, 2019
Monitoring Editor: Saul Purton

The plastid genomes of peridinin-containing dinoflagellates are highly unusual, possessing very few genes, which are located on small chromosomal elements termed "minicircles". These minicircles may contain genes, or no recognisable coding information. Transcripts produced from minicircles may undergo unusual processing events, such as the addition of a 3' poly(U) tail. To date, little is known about the genetic or transcriptional diversity of non-coding sequences in peridinin dinoflagellate plastids. These sequences include empty minicircles, and regions of non-coding DNA in coding minicircles. Here, we present an integrated plastid genome and transcriptome for the model peridinin dinoflagellate *Amphidinium carterae*, identifying a previously undescribed minicircle. We also profile transcripts covering non-coding regions of the *psbA* and *petB/atpA* minicircles. We present evidence that antisense transcripts are produced within the *A. carterae* plastid, but show that these transcripts undergo different end cleavage events from sense transcripts, and do not receive 3' poly(U) tails. The difference in processing events between sense and antisense transcripts may enable the removal of non-coding transcripts from peridinin dinoflagellate plastid transcript pools.

Key words: Plastid genome; minicircles; *A. carterae*; transcript profiling; sense and antisense transcripts.

Introduction

Much is known about the organisation and expression of plastid genomes (Barbrook et al. 2018; Green 2011). The plastid genomes of photosynthetic eukaryotes retain fewer than 250 genes (Green 2011; Muñoz-Gómez et al. 2017); these are typically organised as a single, circular chromosome, although some may have alternative linear or branched forms (Barbrook et al. 2010; Del Cortona et al. 2017; Janouškovec et al. 2013; Oldenburg and Bendich 2004). Genes are usually arranged in operons, and are co-transcribed before being cleaved into mature mRNAs (Barkan 2011; Hotto et al. 2015; Luro et al. 2013). The plastid transcript processing machinery is also involved in the degradation of antisense transcripts (Castandet et al. 2016; Hotto et al. 2015), which may otherwise anneal to and inhibit the function of the corresponding sense transcripts (Hotto et al. 2012; Sharwood

[1]Contributed equally to this work.
[2]Present address: Institut de biologie de l'Ecole normale supérieure (IBENS), Ecole normale supérieure, CNRS, INSERM, PSL Université Paris, 75005 Paris, France
[3]Corresponding author;
e-mail ch26@cam.ac.uk (C.J. Howe).

https://doi.org/10.1016/j.protis.2019.06.001

et al. 2011). These antisense transcripts are generated through transcription from specific promoters located on the plastid template strand (Hotto et al. 2012; Zhelyazkova et al. 2012), through inefficient transcript termination of polymerases transcribing genes that are in opposing transcriptional orientation (Rott et al. 1996; Sharwood et al. 2011), and through RNA-dependent RNA polymerase activity in the plastid (Zandueta-Criado and Bock 2004).

Perhaps the most bizarre example of plastid genome organisation is in the peridinin-containing plastids of dinoflagellate algae (Barbrook et al. 2018). Dinoflagellates are ecologically abundant, and include free-living photosynthesisers, heterotrophs, and endosymbionts of other organisms (Lima-Mendez et al. 2015; Suggett et al. 2017). The majority of the phototrophic species possess a plastid derived from the endosymbiosis of red algae, containing the light-harvesting pigment peridinin (Dorrell et al. 2017; Haxo et al. 1976). The genome of this plastid contains twelve-coding protein genes, two ribosomal RNA genes, and an erratic small number of transfer RNA genes (Barbrook et al. 2014; Mungpakdee et al. 2014), and is fragmented into small circular DNA molecules, termed "minicircles" (Howe et al. 2008; Zhang et al. 1999). Each minicircle contains one gene only, although minicircles with multiple genes are known in individual species (Barbrook et al. 2012; Dorrell et al. 2017; Nelson et al. 2007), alongside a non-coding "core region" that is broadly conserved across all minicircles in a species (Barbrook et al. 2018; Mungpakdee et al. 2014; Nisbet et al. 2004; Zhang et al. 2002). In addition "empty" minicircles and microcircles, which lack coding information, are known in individual dinoflagellate species (Hiller 2001; Nisbet et al. 2004; Zhang et al 1999).

The organisation of the peridinin dinoflagellate plastid genome has influenced the diversity of transcripts produced. Both coding and empty minicircle sequences are transcribed (Nisbet et al. 2008; Wang et al. 2005) through a "rolling circle" mechanism, which can yield transcripts containing multiple copies of plastid minicircle sequence (Barbrook et al. 2012; Dang and Green 2010). However, the predominant bands identified in northern blots of dinoflagellate plastid transcripts correspond to monocistronic mRNAs, which are presumably generated through the processing of these long precursors (Barbrook et al. 2001; Dang and Green 2009; Nisbet et al. 2008). The post-transcriptional processing events observed include cleavage to generate mature transcript 5' and 3' ends (Barbrook et al. 2012; Dang and Green 2010; Dorrell et al. 2016a; Nelson et al. 2007), extensive substitutional editing (Klinger et al. 2018; Mungpakdee et al. 2014; Zauner et al. 2004), and the frequent addition of a 3' poly(U) tail to plastid transcripts (Wang and Morse 2006). Both of the last two processes appear to have evolved within dinoflagellates and their closest evolutionary relatives (e.g. *Chromera*, apicomplexans), independently to other algal chloroplast lineages (Dorrell and Howe 2012; Dorrell et al. 2014; Janouškovec et al. 2010; Nisbet et al. 2016).

We have previously generated extensive plastid sequence data for the model peridinin dinoflagellate *Amphidinium carterae*, including minicircle sequences for all fourteen known dinoflagellate plastid protein-coding and rRNA genes (Barbrook and Howe 2000; Barbrook et al. 2001, 2006, 2018; Nisbet et al. 2004), together with detailed transcript sequence maps generated through RT-PCR and northern blotting of the coding sequences produced from specific plastid minicircles (Barbrook et al. 2012; Dorrell et al. 2017; Nisbet et al. 2008).

Here, we characterise the diversity of non-coding genomic elements and transcripts in the *Amphidinium* plastid. Using integrated genomic and transcriptomic data, we identify a novel, highly transcribed minicircle with no obvious coding content, and profile non-coding transcripts generated from the coding *psbA* and *petB/atpA* minicircles, focussing on transcripts covering minicircle core regions. We also identify the presence of antisense transcripts. Notably, we find that antisense transcripts do not undergo similar terminal cleavage events to those found in mature mRNAs, and lack poly(U) tails. We propose that the differential processing of sense and antisense transcripts in dinoflagellate plastids might indirectly enable the degradation of non-coding sequence degradation during plastid transcript processing.

Results

Coding and Non-coding Diversity of the *Amphidinium carterae* Plastid Genome

First, we wished to produce a definitive inventory of the coding and empty minicircle sequences present in the *Amphidinium carterae* plastid. For this, we performed next-generation sequencing of genomic DNA isolated from *A. carterae* CCMP1314, which had been separated on a caesium chloride gradient (to obtain plastid-enriched DNA) and treated with Plasmid-Safe DNAse (to select for minicircle DNA) to yield a plastid-enriched fraction (Fig. 1) (Griffith 1991; Lang and Burger 2007). We gener-

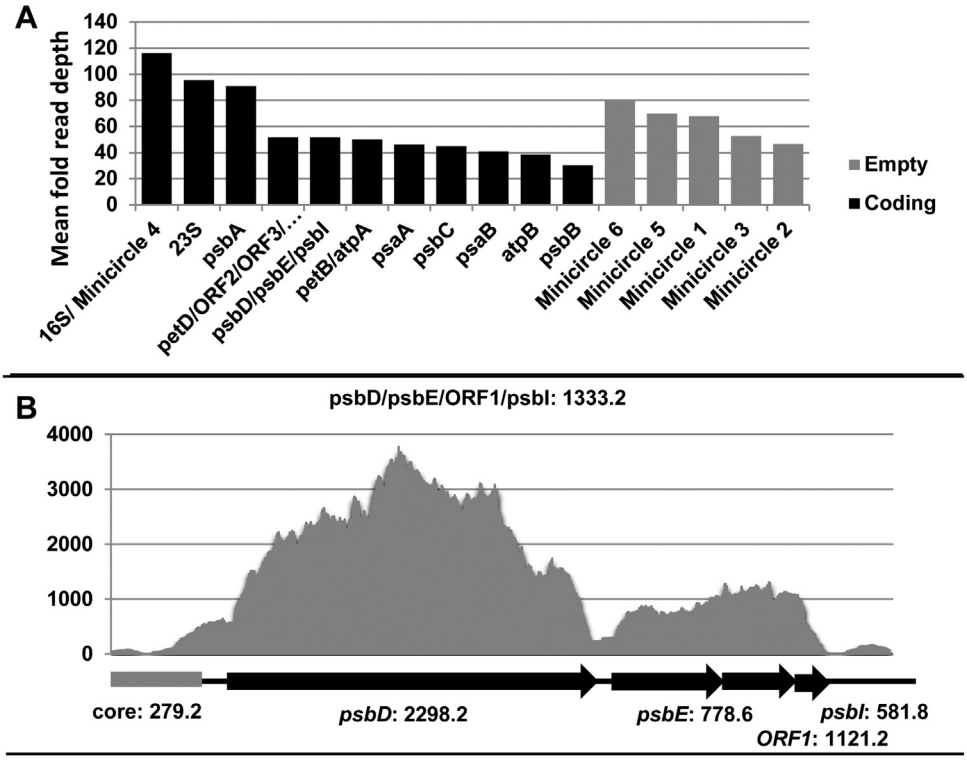

C

Minicircle		CDS	Core	Minicircle		CDS	Core
16S/ minicircle 4	3130.3		96.6	psaB	753.9		14.6
23S	2707.6		6.5	*psaB*		939.1	
atpB	480.7		151.7	psbA	720.4		0.0
atpB		671.5		*psbA*		811.3	
petB-atpA	855.0		8.9	psbB	640.7		74.8
petB		1250.4		*psbB*		950.3	
atpA		1038.6		psbC	421.9		71.4
petD-ORF2-ORF3-ORF4	740.5		185.7	*psbC*		659.3	
petD		1469.6		psbD-psbE-ORF1-psbI	1333.2		146.3
ORF2		1411.7		*psbD*		2298.2	
ORF3		415.0		*psbE*		786.6	
ORF4		183.0		*ORF1*		1121.2	
				psbI		581.8	
Empty minicircle 1	81.6		25.8				
Empty minicircle 2	82.4		14.2	Empty minicircle 5	132.0		53.4
Empty minicircle 3	148.7		78.5	Empty minicircle 6	332.9		36.7

Figure 1. Overview of the *Amphidinium carterae* plastid genome and transcriptome. (**A)** shows all of the minicircle sequences (inferred via the presence of a core region; Barbrook and Howe, 2000), identified from CsCl-enriched *A. carterae* genomic DNA. Identification of orthologous sequences for each minicircle, and PCR verification of the novel empty minicircle sequence, are shown in fig. S1. (**B)** shows an exemplar read coverage plot for the *psbD/psbE/ORF1/psbI* minicircle. This plot shows the total number of reads identified at each position in the minicircle sequence and is shown against a linearised complete minicircle sequence. Thick black arrows correspond to coding sequence, thick grey bars to core sequence, and thin black lines to other non-coding

ated 10,120,479 reads, which we could assemble into 21 minicircle contigs (Supplementary Material Table S1, Sheet 1).

We identified all of the previously identified coding minicircles of the *A. carterae* plastid: *psbA, psbB, psbC, psbD/psbE/psbI, petD, petB/atpA, atpB,* and the 23S minicircle and 16S minicircle (previously annotated as Minicircle 4) (Barbrook and Howe 2000; Barbrook et al. 2001, 2006; Nisbet et al. 2004), with between 30 and 116-fold average read coverage (Fig. 1A). We additionally identified all four of the previously identified "empty" minicircles (Minicircles 1-3 and 5) in *A. carterae* (Nisbet et al. 2004, 2008). These minicircles had comparable (47-80-fold) average read depths to the coding minicircles identified, indicating they form a substantial component of plastid DNA (Fig. 1A). We confirmed that these four empty minicircles lack obvious protein homologues in other sequenced dinoflagellate genomes, and in transcriptome libraries from the Marine Microbial Eukaryote Transcriptome Sequencing Project (MMETSP), supporting the idea that they lack coding function (Supplementary Material Fig. S1A) (Barbrook et al. 2014; Dorrell et al. 2017; Klinger et al. 2018; Mungpakdee et al. 2014). We could not identify distinct equivalents of the "microcircles" (empty minicircles of <1 kbp size) previously sequenced from *A. carterae*, in the genomic dataset, which reflects the fact that these frequently contain sequences identical and indistinguishable from fragments of coding and empty minicircles (Barbrook et al. 2018; Nisbet et al. 2004).

Alongside this, we identified one entirely novel minicircle, referred henceforth as "empty minicircle 6". This corresponded to a 2344 bp empty minicircle sequence, containing 47.7 % GC bases, a value comparable to all existing *A. carterae* minicircle sequences, and a core region including a 9-bp AGAGAAAAA motif conserved in all other minicircle sequences from this strain (Barbrook et al. 2006). We confirmed the presence of this minicircle through PCR and Sanger sequencing from independently isolated *A. carterae* CCMP1314 gDNA (Supplementary Material Fig. S1B). This minicircle was not found to contain any recognisable coding, rRNA or tRNA sequences, either by BLAST or structural searches, nor was it found to contain any regions of sequence similarity to other *Amphidinium* CCMP1314 minicircles (apart from the core region). Instead, it contained an ORF of 163 codons, which is highly similar (>90%) in amino acid sequence to an ORF found on a minicircle previously identified in the related strain *Amphidinium* sp. CS-21 (Hiller 2001), and also similar to a shorter (≥67 aa, C-terminal incomplete) ORF inferred to be encoded by the *Amphidinium massartii* MMETSP transcriptome (Dorrell et al. 2017) (Supplementary Material Fig. S1B). However, the novel ORF generates no significant matches in BLAST searches of protein and translated nucleotide databases outside of the *Amphidinium* genus (Supplementary Material Fig. S1B).We identified transcription of this minicircle in the *A. carterae* CCMP1314 MMETSP library (Supplementary Material Fig. S1A), and through RT-PCR of random-hexamer primed cDNA, but could not identify transcripts from RT-PCRs of oligo-d(A) primed cDNA, using 12 minicircle-specific primers, indicating that this minicircle does not contain any poly(U) sites (Supplementary Material Table S2, section 1, lines 1–18).

Transcriptomic Mapping of the *Amphidinium carterae* Plastid

Next, we wished to determine how abundant the transcripts were from the coding and non-coding sequences contained within the *A. carterae* plastid. We generated a plastid transcriptome for *A. carterae* CCMP1314 by Illumina sequencing of adaptor-conjugated RNA (Supplementary Material Table S1, sheet 2). Each plastid gene was highly represented in the RNA sequence library, with averages of between 3130-fold coverage (for the 16S rRNA) and 581.8-fold coverage (for the photosystem II subunit *psbI*) for each of the recognised genes located in the *A. carterae* plastid genome (Barbrook et al. 2001, 2006; Nisbet et al.

regions of the minicircle. High read coverage is observed over each coding sequence, contrasting with low read coverage in the core region. The intergenic region between *psbD* and *psbE* is demarcated by low read coverage, consistent with *psbD* primarily being processed as a monocistronic transcript in *Amphidinium*, whereas there is a continuous and high read coverage throughout the *psbE-ORF1* and *ORF1-psbI* intergenic regions, consistent with the presence of polycistronic transcripts covering the *psbE-ORF1-psbI* region (Barbrook et al. 2012). Additional read coverage plots are supplied in fig. S2. (**C)** tabulates the average read coverage for the complete sequences of each *Amphidinium* plastid minicircle with verified coding content, along with the core regions of each minicircle, and each confirmed open reading frame present.

2004) (Fig. 1B, C). We observed very little relative difference in the transcript abundance of each plastid gene (Fig. 1C). This is in contrast to what is observed in other alveolate plastid transcriptomes (e.g. *Chromera velia* and *Karenia mikimotoi;* (Janouškovec et al. 2013; Dorrell et al. 2016a)), where transcripts encoding the photosystem II reaction centre subunits *psbA* and *psbD* are far more abundant than those from other plastid genes. We notably found higher transcript read coverage on the novel empty minicircle 6 (332.9) compared to other empty minicircles (81.6–148.7; Fig. 1C), consistent with the fact that this was the only empty minicircle detectable in the *A. carterae* MMETSP transcriptome (Supplementary Material Fig. S1C).

We noted varying patterns of read coverage for different minicircles, consistent with different patterns of transcript maturation (Fig. 1B; Supplementary Material Fig. S2). For example, the *psbE, ORF1* and *psbI* genes, which are adjacent to one another in the *psbD/psbE/ORF1/psbI* minicircle, showed similar levels of read coverage with no clear decrease in coverage over the intergenic region, reinforcing previous evidence that they are cotranscribed and processed to form a polycistronic transcript (Barbrook et al. 2012) (Fig. 1B). We similarly observed largely continuous read coverage between *petD* and *ORF2* in the polycistronic *petD/ORF2/ORF3/ORF4* minicircle, consistent with previous RT-PCR data indicating that these genes are cotranscribed and possess a common poly(U) site, located downstream of ORF2 (Barbrook et al. 2012) (Supplementary Material Fig. S2).

In contrast, *psbD* which has been shown to be processed to a monocistronic transcript, was covered by a clearly defined pattern of associated reads (Fig. 1B) (Barbrook et al. 2012; Nisbet et al. 2008). We similarly observed defined gaps in read coverage between *petB* and *atpA* in the polycistronic *petB/ atpA* minicircle; and between *petD/ORF2* and *ORF3* in the *petD/ORF2/ORF3/ORF4* minicircle consistent with previous northern and RT-PCR data indicating these genes are represented by separate mRNA populations (Barbrook et al. 2001, 2012) (Supplementary Material Fig. S2).

Elsewhere, the mRNA sequencing data provided windows into the processing events associated with previously unexplored *Amphidinium* plastid genes (Supplementary Material Fig. S2). These included substantial read coverage within the *petD* and *atpB* 5' UTRs, despite the fact that the 5' end of each gene is marked by a defined minimum in transcript coverage; these might plausibly correspond to previously undetected plastid ORFs, or regions encoding small RNAs. Moreover, we detected maximal coverage of over 6000 and 16000-fold respectively in the 23S and 16S minicircles, despite other presumed coding regions of both minicircles having substantially below 1000-fold read coverage (Supplementary Material Fig. S2). Alongside previous data suggesting that the 23S and 16S sequences of dinoflagellate plastids are highly divergent and lack otherwise conserved regions, these peaks might be consistent with internal cleavage of ribosomal RNAs into topographically separate elements (Barbrook et al. 2006; Dang and Green 2009). Verification of these peaks, by northern blotting or RT-PCR, will be essential to determine if they reflect genuine transcript processing events, or reflect secondary structures or other features within plastid mRNA pools.

Terminal Processing of Non-coding and Core-containing Transcripts of Plastid Minicircles

For all minicircles studied, we noted that there were very few reads covering non-coding sequences such as core regions. For example, in the case of the *psbD-psbE-ORF1-psbI* minicircle, which had an average 1333-fold read coverage over the entire sequence, and a maximum 3778-fold read coverage within the *psbD* CDS, the average read coverage for the 280 bp core region (Barbrook and Howe 2000) was 146-fold, with a minimum of 3-fold coverage within the core interior (Fig. 1B). We found similar scenarios in all other minicircles studied (Fig. 1B). This supports evidence from previous studies that transcripts covering minicircle core regions are present at only very low abundance in dinoflagellate plastid RNA pools (Barbrook et al. 2012; Dang and Green 2010; Nisbet et al. 2008).

We have previously characterised the mature coding transcripts produced from each minicircle both by northern blotting, and RT-PCR (Barbrook et al. 2001, 2012). We now wished to investigate what terminal processing events are associated with non-coding and core-containing transcripts. First, we hybridised northern blots of total cellular RNA using single-stranded RNA probes complementary to different regions of the *psbA* and *petB/atpA* minicircles (Fig. 2A, B; Supplementary Material Table S5, probes labeled "sense" in column B), including non-coding regions (the *petB* 5' UTR, and the *psbA* 5' and 3' UTR) and coding regions of each minicircle. To visualise the non-coding transcript diversity of each minicircle, we

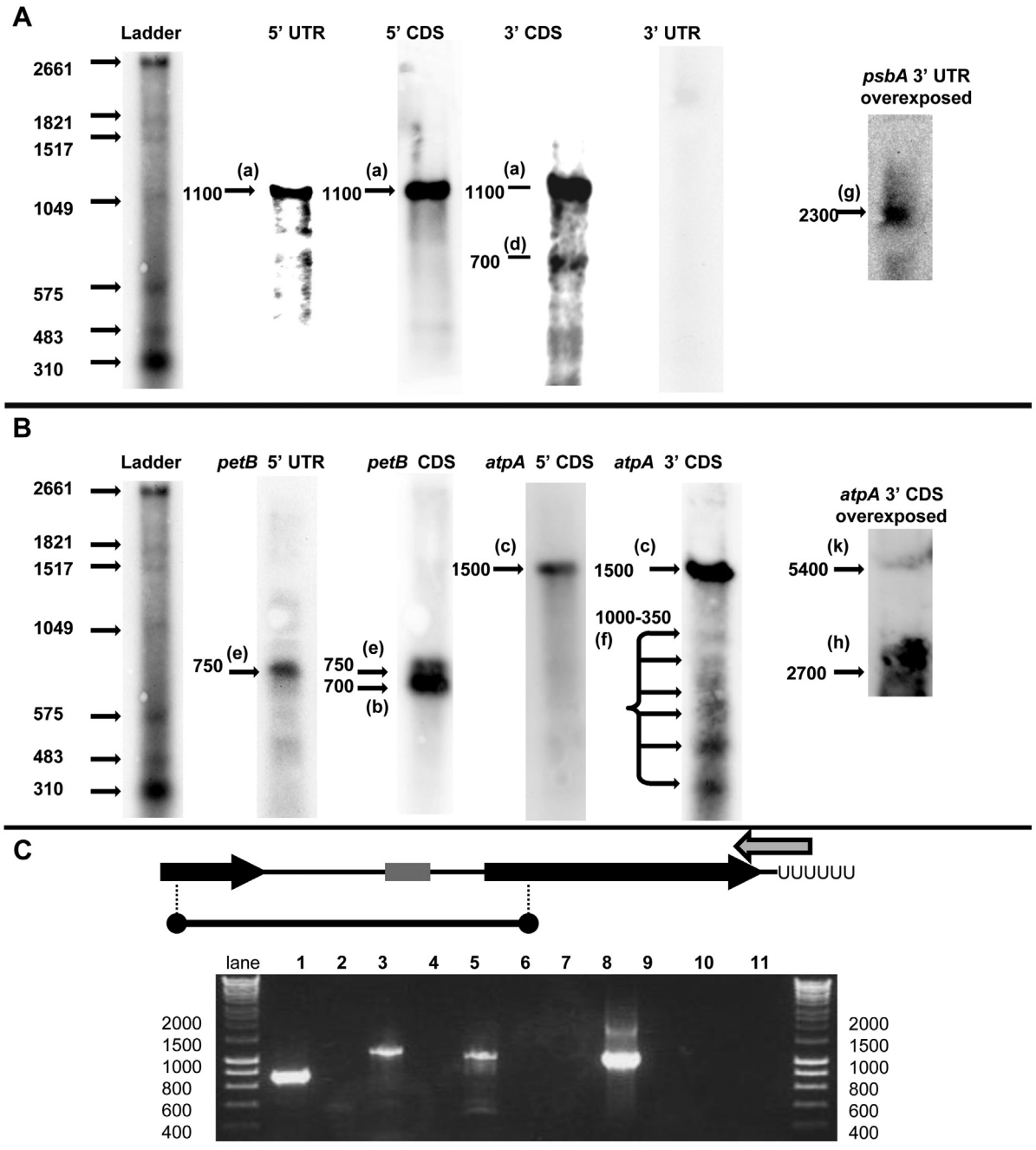

Figure 2. Diversity of multi-copy and core-containing transcripts. (**A**) and (**B**) show northern blots hybridised with single-stranded RNA probes complementary to different regions of coding strand sequences, respectively from the *psbA* **(A)** and *petB/atpA* **(B)** minicircles. Key bands are identified with arrows. Sizes of each band were calculated by comparison to a DIG-labelled RNA ladder separated on the same gel. Transcripts a–c represent the predominant, monocistronic mRNAs produced from each gene, as identified by comparison to transcript sizes estimated from previous northern blot and circular RT-PCR studies (Barbrook et al. 2001, 2012); and transcripts d-f represent lower abundance bands of less than one minicircle length. Corresponding circular RT-PCR experiments are shown in Supplementary Material Figure S3. (**C**) shows RT-PCRs employed to detect polyuridylylated multi-copy transcripts from the *A. carterae psbA* and *petB/atpA* minicircles. (Top) a putative transcript of a hypothetical minicircle is shown. The black arrow corresponds to all coding regions present within the minicircle, i.e. either one gene (for monocistronic minicircles) or multiple gene sequences (for polycistronic

used much larger quantities of total cellular RNA (30 μg) than previously hybridised.

The most intense hybridisation obtained corresponded in size to the monocistronic mRNAs of each gene (transcripts labelled a–c; *psbA*: 1100 nt, *petB*: 700 nt, *atpA*: 1500 nt; Fig. 2A, B). We additionally identified lower abundance bands of less than one minicircle length (transcripts labeled d–f; *psbA*: 700 nt, *petB*: 750 nt, *atpA*: 1000–350 nt). We could additionally detect, in overexposed *psbA* blots, a 2300 nt transcript (band labeled g, Fig. 2A); and 2700 and 5400 nt transcripts in overexposed *petB/atpA* blots (bands labeled h, k; Fig. 2B). As the length of the *psbA* and *petB/atpA* minicircles are respectively 2311 bp and 2713 bp, these transcripts are likely to correspond to transcripts containing one, or two complete minicircle sequences.

Alongside this, we performed circular RT-PCR, a technique that allows the precise identification of 5' and 3' terminus positions from individual transcripts (Barbrook et al. 2012). For this, cDNA synthesis was carried out using primers specific to core regions of the *psbA* and *petB/atpA* minicircles, and PCR reactions were then performed using different combinations of primers, designed against different regions of minicircle sequence, to identify core-containing transcripts present (see Methods) (Supplementary Material Fig. S3A; Table S2, section 2, lines 19–41).

26 core-containing transcripts were identified through this approach (Supplementary Material Fig. S3B; Table S3, sections 1–2, lines 5–57). Twenty of the transcripts that were identified (13 from the *psbA* minicircle, 7 from *petB/atpA*) were less than one minicircle in length. These transcripts terminated at the 3' end within the minicircle core region, and none contained a complete coding sequence. The remaining six transcripts (5 from *petB/atpA*, and one *psbA* transcript) were of greater than one minicircle length, thus corresponding to multi-copy transcripts (Supplementary Material Fig. S3B; Table S3, sections 1–2, transcripts marked "multi-copy" in column A). The multi-copy *psbA* transcript extended through a complete copy of *psbA* downstream of the core region, terminating in the *psbA* 3' UTR (Supplementary Material Table S3, section 1, line 13); and all five of the multi-copy *petB/atpA* transcripts contained a complete downstream copy of *petB,* although in each case they terminated at the 3' end within the *atpA* CDS, hence did not have a complete downstream *atpA* sequence (Supplementary Material Table S3, section 2, lines 44–48).

Two of the multi-copy transcripts from the *petB/atpA* minicircle had similar 5' ends to those identified for monocistronic, polyuridylylated *atpA* mRNAs, located 340 and 345 bp upstream of the *atpA* CDS (Fig. S3B, asterisked *petB/atpA* multi-copy transcripts ii and iii; Supplementary Material Table S3, section 2, lines 45–46). Similar 5' end positions for monocistronic *atpA* transcripts have also been identified in previous circular RT-PCR studies (Barbrook et al. 2012). Thus, some core-containing transcripts undergo similar cleavage events generating 5' ends as monocistronic mRNAs.

Core-containing Transcripts Can Receive poly(U) Tails

Given the presence of mature 5' ends on some core-containing transcripts, we wished to determine whether core-containing transcripts ever receive 3' poly(U) tails. As we did not detect polyuridylylated core-containing transcripts by circular RT-PCR, we performed an oligo-d(A) primed RT-PCR to investigate directly their presence for

circles); and the core region as a box. A cDNA synthesis primer (grey arrow) was designed containing a 5' oligo-d(A) region, and a 3' region complementary to the 3' UTR sequence region directly upstream of either the *psbA, petB* or *atpA* poly(U) site. PCRs (below) were performed using the cDNA and pairs of PCR primers that flank the cDNA primer annealing site. These reactions will specifically amplify polyuridylylated transcripts that additionally contain a second copy of minicircle sequence. The gel photograph (bottom) shows products as following. Lane **1**: RT-PCR to detect polyuridylylated multi-copy transcripts from the *petB/atpA* minicircle using a cDNA synthesis primer specific to the *petB* poly(U) site. Lane **2**: reverse transcriptase negative control for lane 1. Lane **3**: RT-PCR to detect polyuridylylated multi-copy transcripts using a cDNA synthesis primer specific to the *atpA* poly(U) site. Lane **4**: reverse transcriptase negative control for lane 3. Lane **5**: RT-PCR to detect polyuridylylated multi-copy transcripts from the *psbA* minicircle. Lane **6**: reverse transcriptase negative control for lane 5. Lane **7**: blank lane. Lane **8**: reaction positive control, using a genomic DNA template and PCR primers internal to the *psbA* CDS. Lanes **9–11**: RT-PCRs using the *psbA*, *petB* and *atpA* poly(U) site cDNA synthesis primers respectively, and PCR primers internal to the *petB* (lane 9) and *psbA* (lanes 10, 11) CDS, confirming the minicircle specificity of cDNA synthesis.

the *petB/atpA* and *psbA* minicircles. First, cDNA was synthesised using primers containing an oligo-d(A) sequence at its 5' end, and a gene-specific sequence at the 3' end of two minicircles (encoding *petB/atpA* and *psbA*; Supplementary Material Table S2, section 3, lines 45–47) (Barbrook et al. 2012). Each primer would therefore specifically anneal to transcripts containing a 3' poly(U) tail (through complementary pairing to the oligo-d(A) region), but should preferentially anneal to transcripts of the gene corresponding to the gene-specific region. PCR amplifications of the generated cDNA were performed using combinations of primers flanking the cDNA synthesis site, to identify transcripts that contained a second copy of the minicircle CDS (Fig. 2C; Supplementary Material Table S2, section 3, lines 48–54).

For all three genes, products were identified consistent with the presence of polyuridylylated multi-copy transcripts (Fig. 2C; lanes 1, 3, 5). Products were not identified for any PCR under reverse transcriptase negative conditions, confirming that these products were not due to residual gDNA contamination (Fig. 2C; lanes 2, 4, 6). To confirm that the cDNA primers employed annealed specifically to polyuridylylated transcripts of one gene, PCRs were performed using template generated with the *psbA* cDNA primer and the *petB* PCR primers, and using template generated with either the *petB* or *atpA* primer and the *psbA* PCR primers (Fig. 2C; lanes 9–11). Products were not identified in any case, confirming that the cDNA primers used were specific to the intended template, and were not annealing to other transcripts in the RNA samples at detectable levels. Thus, poly(U) tails can be added to RNA transcripts of more than one minicircle length.

Presence of Antisense Transcripts in Peridinin Dinoflagellate Plastids

We wished to test whether antisense transcripts were present in the *A. carterae* plastid. The RNA library used for sequencing was ligated to a custom RNA adapter prior to cDNA synthesis, allowing the precise identification of transcript termini (Supplementary Material Fig. S4A) (Dorrell et al. 2016a; Scotto-Lavino et al. 2006). As this RNA adapter was non-palindromic, it can be used to discriminate sense and antisense transcripts, i.e. by comparing the orientation of the ligation site to the the corresponding minicircle sequence (Supplementary Material Fig. S4A). We therefore inspected the next-generation sequence data for evidence of antisense transcripts. We found 955 reads that contained a detectable transcript 5' end, of which 67 (7.0%) corresponded to transcripts in the reverse orientation of the minicircle sequence, i.e. possible plastid antisense transcripts (Supplementary Material Fig. S4 and Table S4) (Dorrell et al. 2016a; Georg et al. 2010). We detected only negligible numbers of plastid transcript 3' end ligation sites through this approach (data not shown).

We additionally searched for antisense transcripts using RNA-ligase mediated 5' RACE. This technique uses the same RNA adapter ligation previously used for the next-generation sequencing experiments. However, in this case, cDNA was synthesised from adapter ligated *A. carterae* RNA using primers with the same sequence as the coding strands of the *psbA* and *petB/atpA* minicircles (Supplementary Material Fig. S4A; Table S2, section 4, lines 57–59), which would anneal to antisense transcripts. These cDNA products were used as template for PCRs, using primers with the same sequence as the coding strand of the *psbA* and *atpA* genes, and a PCR primer with the same sequence as the RNA adapter used (Supplementary Material Fig. S4A; Table S2, section 4, lines 61–63).

Through this approach, we detected an antisense transcript for the *atpA* gene, which terminated at the 5' end at a position 115 bp inside the 5' end of the *atpA* (Supplementary Material Fig. S4C). This product was detected independently three times, using different RNA samples, but could not be identified in ligation- or reverse-transcriptase negative controls, confirming that it was not an artifact of mis-annealing of the adapter-specific primer on similar regions of minicircle sequence, or the result of genomic contamination in the adapted RNA libraries.

Finally, we performed RT-PCRs using the antisense cDNA preparations, the primer used for cDNA synthesis, and a PCR primer designed to be similar to the spliced-leader (SL) sequence, a short motif associated with the 5' end of most dinoflagellate nuclear transcripts (Gavelis et al. 2015; Lin et al. 2010). Products were not detected, suggesting that it is unlikely that these transcripts were generated within the dinoflagellate nucleus.

Antisense Transcripts are not Complementary to Sense Transcripts

In plants, and in the fucoxanthin-containing dinoflagellate *Karenia mikimotoi*, sense and antisense transcripts from individual plastid genes

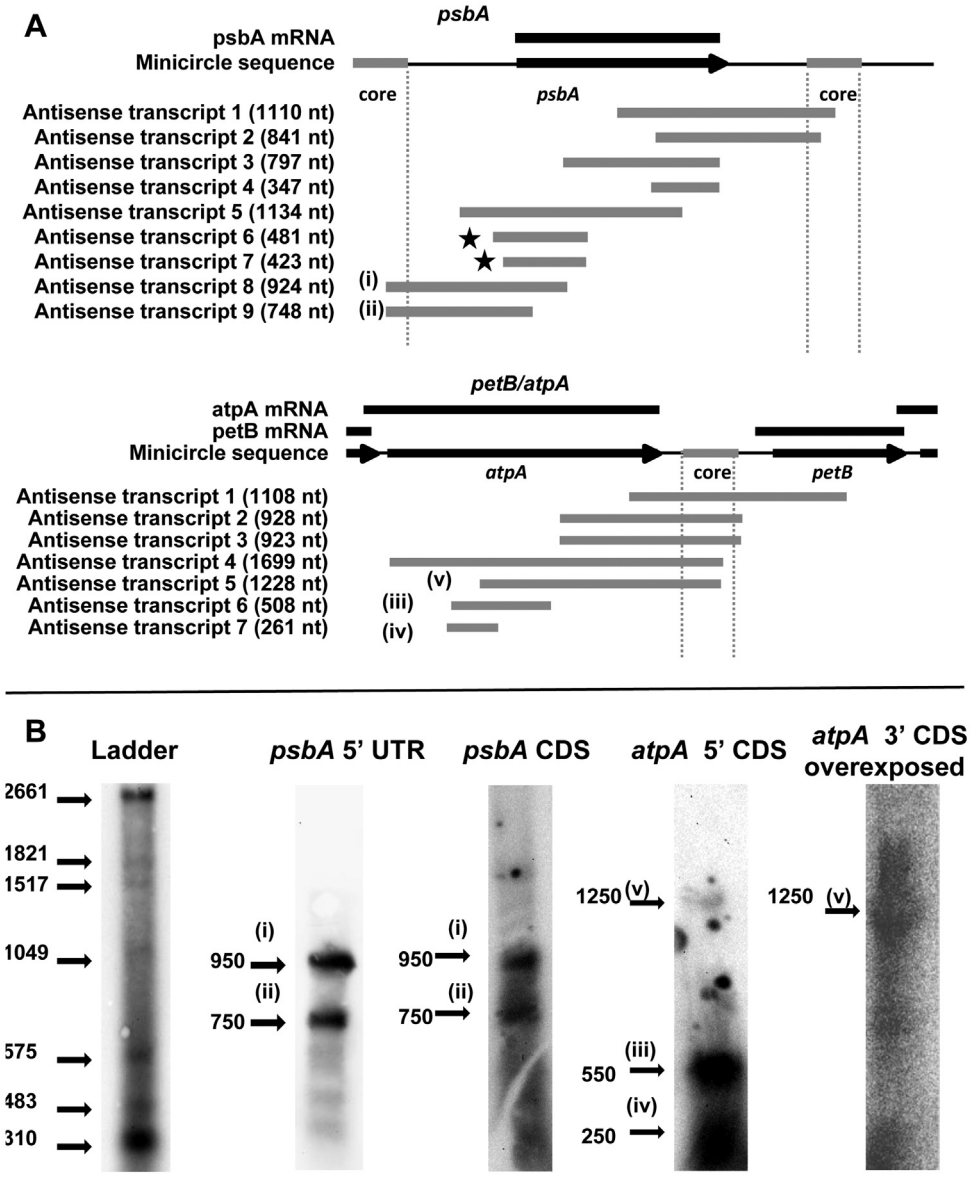

Figure 3. Circular RT-PCR and northern blots of *psbA* and *petB/atpA* minicircle antisense transcripts. (**A**) shows the diversity of antisense transcript termini mapped by circular RT-PCR for the *psbA* and *petB/atpA* minicircles. Transcripts are displayed on transcript diagrams against a linearised hypothetical sense transcript of each minicircle, shown as per Fig. 1. Transcript sequences that terminate at the same positions as mature mRNA sequences are labelled with asterisks. Transcript sequences that correspond to bands identified in northern blots of antisense transcripts, are labelled with brackets. Antisense transcript termini identified through next-generation sequencing, and 5' RACE, are shown in Supplementary Material Figure S4. (**B**) shows the results of northern blots hybridised with single-stranded RNA probes complementary to different regions of template strand sequence to detect antisense transcripts, as Fig. 2A, and B. Each antisense transcript band is labelled with a number corresponding to probable matching transcripts in the circular RT-PCR experiment above. Probes complementary to antisense transcripts covering the *psbA* CDS 3' end and 3' UTR, and the *petB* CDS and 5' UTR, failed to yield any distinct bands, the corresponding blots are not shown. As the *atpA* 3' CDS blot only produced very weak fluorescence, an overexposed blot image is shown.

have been documented to possess different consensus terminus positions (Dorrell et al. 2016a; Zghidi-Abouzid et al. 2011). We tested whether this is true also in *A. carterae* by detailed profiling of the predominant terminus positions associated with sense and antisense transcripts over the *A. carterae psbA* and *petB/atpA* minicircles. First, we performed circular RT-PCR using cDNA synthesis primers complementary to the template strand of each minicircle, and PCRs using different combinations of primers, against different regions of each minicircle sequence, to obtain an estimate for the full diversity of antisense transcripts that are present (Fig. 3A; Supplementary Material Table S2, section 5, lines 65–83). We additionally hybridised northern blots with single-stranded RNA probes with the same sequence as regions of each minicircle coding strand, to identify the antisense transcripts associated with regions of each minicircle complementary to previously investigated sense transcripts (Figs 2A, B, 3B; Supplementary Material Table S5, probes labeled "antisense" in column B).

We identified multiple potential antisense transcripts from each minicircle through each approach. The vast majority of antisense transcripts identified by circular RT-PCR terminated at positions distinct from the corresponding sense transcripts from each minicircle (Fig. 3A; Supplementary Material Table S3, sections 3, 4, lines 59–95). For example, we could not identify any antisense transcripts that terminated at either ends at positions complementary to the *psbA, petB* or *atpA* poly(U) sites, and only found two that might possess termini complementary to consensus mRNA 5' end positions (Fig. 3A, asterisked transcripts; Supplementary Material Table S3, section 3, lines 73–74).

For the *psbA* minicircle, two transcripts, of 750 nt and 950 nt length, were detected by northern blot using probes for the 5' UTR and 5' end of the CDS (Fig. 3B; transcripts labeled i–ii). These may correspond to two antisense transcripts, one 748 nt length, and one 924 nt length, identified through circular RT-PCR (Fig. 3A). For the *petB/atpA* minicircle the predominant bands were identified for *atpA* (of 250 and 500 nt length) with the 5' end probe (Fig. 3B; transcripts labelled iii–iv). These may correspond to 261 nt and 508 nt length antisense transcripts identified by circular RT-PCR, covering regions internal to the *atpA* CDS (Fig. 3A, B; transcripts labelled iii, iv). A faint band of approximately 1250 nt length was identified on overexposure of the blots hybridised to both the 5' and 3' *atpA* probes, which may correspond to a 1228 nt transcript identified from circular RT-PCR to extend from the core into the region complementary to the 5' end of *atpA* (Fig. 3A, B; transcript labelled v).

In no case did we identify northern hybridization in an antisense transcript blot of the size corresponding to a mature mRNA (i.e., an 1100 nt *psbA* transcript, a 700 nt *petB* transcript, or a 1500 nt *atpA* transcript), or a visualized non-coding or core-containing transcript (e.g., transcripts corresponding to one or two complete minicircle lengths) from the sense strand blots (Figs 2A, B, 3B). Moreover, we did not identify any hybridisation in the *psbA* blots that might correspond to the two antisense transcripts identified through circular PCR with terminus positions complementary to sense transcripts (expected transcript size 400–500 nt; Fig. 3A, B). Thus, sense and antisense transcripts undergo different terminal processing events in the *A. carterae* plastid.

Antisense Transcripts Lack poly(U) Tails

We wished to determine whether poly(U) tail addition in peridinin dinoflagellates is preferentially associated with sense transcripts over antisense transcripts, as occurs in the fucoxanthin-containing species *Karenia mikimotoi*. To do this, cDNA was synthesised from *A. carterae* total cellular RNA using an oligo-d(A) primer previously shown to anneal to plastid poly(U) tails from a wide range of plastid genes in dinoflagellate and related species (Supplementary Material Table S2, section 6, line 86) (Barbrook et al. 2012; Dorrell and Howe 2012; Dorrell et al. 2014; Richardson et al. 2014). PCRs were then performed using the same oligo-d(A) primer as a PCR primer, paired with a PCR primer with the same sequence as the template strands of the *psbA* and *petB/atpA* minicircles, to identify polyuridylylated antisense transcripts (Supplementary Material Table S2, section 6, lines 88–95).

Products were not identified using any of the template strand primers, indicating that polyuridylylated antisense transcripts were not present (Fig. 4; lanes 2–3, 7–8). Products were not detected even following a second round of PCR amplification of the primary PCR product. In contrast, polyuridylylated sense transcripts were amplified from each cDNA preparation, by PCR with the oligo-d(A) primer, and PCR primers with the same sequence as the coding strand of the *psbA*, *petB* and *atpA* genes, confirming that the oligo-d(A) primed cDNA synthesis reactions were successful (Fig. 4; lanes 4, 9, 10). In addition, products covering each of the regions of sequence tested were amplified from each RNA sample, using gene-specific cDNA syn-

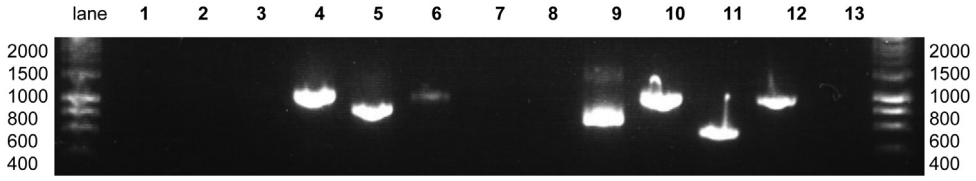

Figure 4. Absence of poly(U) tails from antisense transcripts. This gel photograph shows the result of a series of RT-PCRs to test for poly(U) tails on antisense transcripts of the *psbA* and *petB/atpA* minicircles. Lanes 1, 13: blank lane. Lanes 2–3, 7–8: RT-PCRs performed with an oligo-d(A) primer for cDNA synthesis, and PCR with the same oligo-d(A) primer and a primer with the same sequence as the template strand of the *psbA* CDS (2) and UTR (3), and the *petB* (7) and *atpA* CDS (8), demonstrating the absence of polyuridylylated antisense transcripts extending over these regions. Lanes 4, 9–10: RT-PCR performed with oligo-d(A) primed cDNA as before, and PCR with oligo-d(A) and primers with the same sequence as the coding strands of the *psbA* (4), *petB* (9) and *atpA* CDS (10), confirming the presence of polyuridylylated sense transcripts in the RNA sample. Lanes 5, 6, 11, 12: positive controls for the presence of antisense transcripts over the *psbA* CDS (5) and UTR (6), and the *petB* (11) and *atpA* CDS (12), using a gene-specific cDNA synthesis and PCR primer with the same sequence as the coding strands of minicircle sequence, and the same template strand PCR primer as used in the corresponding oligo-d(A) primed PCR for each reaction.

thesis and PCR primers (Fig. 4, lanes 5–6; 11–12). Thus, antisense transcripts of the *psbA* and *petB/atpA* minicircles in the *A. carterae* plastid do not possess 3' poly(U) tails.

Discussion

We have produced a comprehensive study of the plastid genome and transcriptome of the model peridinin-containing dinoflagellate species *Amphidinium carterae*. We show that existing surveys of the coding and non-coding diversity of this genome (Barbrook et al. 2018) are largely complete, although we document a previously unidentified non-coding minicircle from next-generation sequencing (Fig. 1). Unusually, transcripts from this minicircle are at somewhat higher abundance than other empty minicircles, and it contains an ORF also detectable in other members of the genus *Amphidinium* (Supplementary Material Figs S1, S2); whether this is consistent with it possessing a coding or other function remains to be determined. Otherwise, we demonstrate that the peridinin dinoflagellate plastid is characterised by relatively uniform transcript abundance across all protein coding regions (Fig. 1; Supplementary Material Fig. S2). This is consistent with differences in gene expression being mediated by post-transcriptional or translational regulation, as has previously been inferred to occur both at specific dinoflagellate plastid loci, and in the dinoflagellate nucleus (Okamoto and Hastings 2003; Wang et al. 2005).

Our data indicate that core-containing, and non-coding regions of minicircle sequence are present at much lower abundance in plastid transcript pools than coding sequences (Figs 1B, C; Supplementary Figure S2), consistent with information from previous studies (Barbrook et al. 2012; Dang and Green 2010; Nisbet et al. 2008). The low read coverage over minicircle core regions might reflect limited transcription through these sequences, for example if the minicircle core acts as an effective transcriptional terminator, or alternatively might reflect very efficient cleavage or degradation of multi-copy transcripts by the plastid transcript processing machinery (Dang and Green 2010; Nisbet et al. 2008). Notably, we infer the presence of both mature 5' end processing sites, and 3' poly(U) tails on some core-containing transcripts of more than one minicircle length (Fig. 2C; Supplementary Material Fig. S3). Polyuridylylated polycistronic transcripts of less than one minicircle length have additionally previously been identified from the multigene *petB/atpA* and *psbD/psbE/psbI A. carterae* minicircles (Barbrook et al. 2012; Nisbet et al. 2008). These long transcripts with mature 5' and 3' termini in peridinin plastids might represent processing precursors of mature mRNAs, or might equally represent mis-processed transcripts generated as a result of inefficient end cleavage or transcript termination in peridinin plastids.

Finally, we have identified antisense transcripts from the *A. carterae psbA* and *petB/atpA* minicircles (Figs 3, 4; Supplementary Material Fig. S4), similar to those previously identified in the plastids of plants (Castandet et al. 2016; Georg et al. 2010), apicomplexans (Bahl et al. 2010; Nisbet et al. 2016), and fucoxanthin-containing dinoflagellates (Dorrell et al. 2016a). It remains to be determined how these transcripts are generated. We do not identify 3' poly(A) tails, nor 5' spliced leader sequences on

any antisense transcript, which might be applied if they were products that had been expressed from previously plastid gene fragments, which have been relocated to the nucleus (Gavelis et al. 2015; Lin et al. 2010; Owari et al. 2014). Moreover, the antisense transcripts do not have complementary terminus positions to those associated with mature mRNAs for each minicircle (Figs 2, 3), which suggests that they are not the products of a direct RNA-dependent RNA polymerase activity on sense plastid transcripts (Zandueta-Criado and Bock 2004). Thus, we tentatively propose that the antisense transcripts are generated through the transcription of plastid minicircle coding DNA strands. This may be through the activity of specific promoters located in the reverse orientation, or through transcription initiation events that are not dependent on specific primary sequence motifs, with the plastid RNA polymerase recruited to features such as stem loops or single-stranded nicks in minicircle sequence (Barbrook et al. 2018; Dang and Green 2009; Leung and Wong 2009; Zhang et al. 2002). Verifying this will require detailed mapping of promoter sequences in dinoflagellate plastids, for example through high-throughput techniques such as dRNA-seq (Zhelyazkova et al. 2012).

It remains to be determined whether antisense transcripts possess specific functions in dinoflagellate plastids. In plants, the accumulation of antisense plastid transcripts appears to vary in response to thermal stress (Castandet et al. 2016; Georg et al. 2010). Plastid antisense transcripts might therefore have regulatory effects, constraining the processing and expression of sense transcripts in response to environmental and physiological changes, similar to the functions of miRNAs in nuclear genomes (Fujii et al. 2005). Alternatively, antisense transcripts might have purely deleterious effects on transcript processing and translation efficiency, and be actively removed from plastid transcript pools, as has also been documented in plants (Castandet et al. 2013; Hotto et al. 2015; Sharwood et al. 2011). In this latter regard, we note that the antisense transcripts in the *A. carterae* plastid appear to be present at low abundance (Fig. 3; Supplementary Material Fig. S4), as is the case in fucoxanthin dinoflagellate and apicomplexan plastids (Dorrell et al. 2016a; Nisbet et al. 2016) and do not receive 3' poly(U) tails (Fig. 4). Previous studies have suggested that the poly(U) tail confers 3' end stability to plastid transcripts in dinoflagellates and related species (Barbrook et al. 2012; Dang and Green 2009; Dorrell et al. 2014; Janouškovec et al. 2013). The specific addition of a poly(U) tail to sense transcripts during transcript processing might therefore enable antisense transcripts to be preferentially degraded, leaving a plastid transcript pool enriched in mature mRNAs.

Concluding Remarks

Control of dinoflagellate plastid gene expression and physiology is clearly complex, relying on both transcriptional control and post-transcriptional processing events (Nassoury et al. 2005; Wang et al. 2005), and different processing events may distinguish mature mRNAs from non-coding transcripts (Dorrell et al. 2016b; Richardson et al. 2014). Understanding the functional significance of antisense transcripts, and their associated processing events, will depend on being able to manipulate dinoflagellate plastid genomes, e.g. through the introduction of transgenic minicircles producing antisense transcripts, which is now possible (Nimmo et al. 2019). Genetic manipulation of plastid genome content and gene expression in dinoflagellates may provide fresh insights into the unusual transcript processing events associated with this lineage.

Methods

Cultures and nucleic acid isolation: *Amphidinium carterae* CCMP 1314 was cultured in f/2 medium, which was prepared with Ultramarine Synthetica artificial sea water (Waterlife) and buffered with 500 μg/ml tricine to pH 8, under a 12:12 light: dark cycle, at 30 $\mu E\ m^{-2}\ s^{-1}$ illumination, at 20 °C, without shaking.

DNA from *A. carterae* was purified by phase separation with phenol: chloroform, followed by ethidium bromide-caesium chloride gradient centrifugation, following previous methodology (Barbrook and Howe 2000). The fraction corresponding to minicircle DNA was removed with a needle. Purified and cleaned DNA (1 μg) was treated with 10U Plasmid-Safe ATP-dependent DNase (Lucigen) overnight. The DNA was purified using a phenol-chloroform extraction retaining the aqueous phase, precipitated with ethanol and sodium acetate. The pellet was washed with 70% ethanol, air dried and resuspended in TE buffer, pH 8.0.

RNA was extracted using Trizol (Invitrogen), following previous methodology (Barbrook et al. 2012), treated with DNase I (Qiagen), and cleaned with an RNeasy column (Qiagen), following the manufacturer's instructions. The integrity of cleaned RNA samples was confirmed following electrophoresis on RNase-free TBE-agarose gels, and RNA samples were confirmed to be free of residual DNA contamination via two rounds of PCR, in the absence of reverse transcription, using PCR primers against consensus regions of the nuclear 18S and ITS1 sequences (Gachon et al. 2013). All nucleic acid concentrations were confirmed with a Nanodrop spectrophotometer.

Genome sequencing: Isolated *Amphidinium* DNA was sequenced using a NextSeq500 machine (Illumina) in single-

read mode, running 150 cycles, by the sequencing facility in the Biochemistry Department, University of Cambridge. 10,120,479 reads of 151 bp length were generated. The quality of these reads was checked using Fast QC (Blankenberg et al. 2010). Reads were then trimmed from base 5 to 135. Multiple *de novo* assemblies were made using Unicycler (Wick et al. 2017), utilising the trimmed sequences. Inspection of the alignments revealed there was contamination from *A. carterae* mitochondrial DNA and from *Bacillus oceanisediminis*. All assemblies of 3300 bp and smaller were examined. The Fast QC, trimming and assemblies were performed using the Galaxy web interface (Blankenberg et al. 2010). This library has been deposited in NCBI SRA (ID: PRJNA524783).

Twenty-one minicircle contigs were identified through this approach, including four that mapped as circular. The sequence of one novel potential minicircle was confirmed by PCR and Sanger DNA sequencing, using a custom set of twelve gene-specific primers (Supplementary Material Table S2, section 1, lines 1–16). The orthology and evolutionary conservation of minicircle sequences in different dinoflagellate species was assessed by tBLASTx search, with threshold evalue 1×10^{-05}, against this and all other dinoflagellate species sequenced as part of MMETSP, followed by verification through a reciprocal BLASTx search against nr, following previous methodology (Dorrell et al. 2017). Potential coding functions were assessed in novel minicircle sequences by BLAST search against the nr database; and potential tRNA sequences were searched for using tRNAscan-SE and Aragorn (Laslett and Canback 2004; Lowe and Eddy 1997; Nelson et al. 2007). The novel minicircle sequence has been deposited in GenBank (ID: MK598758-MK598759), and is additionally provided in Supplementary Material Table S1, sheet 4.

Transcriptome sequencing: Transcriptome sequencing was performed using adapter-ligated total cellular RNA, generated by incubation of 1 μg DNA-free total cellular RNA from *Amphidinium carterae*, with 1 μg of a custom RNA adapter (GCUGAUGGCGAUGAGCACUGGGUUGCAA) using T4 RNA ligase (Promega) as previously described (Dorrell et al. 2016a). The ligation products were cleaned with an RNeasy column (Qiagen) and eluted in 30 μl DEPC-treated water. 10 μl of the eluted product was used as template for synthesis with a Maxima H Minus double stranded cDNA synthesis kit (Thermo), per the manufacturer's instructions. The product of the cDNA synthesis reaction was cleaned using a MinElute cleanup column (Qiagen), and eluted in a further 30 μl DEPC-treated water.

Double stranded cDNA was quantified using a Qubit fluorometer (Invitrogen) following the manufacturer's instructions. A sequencing library was generated from 100 ng purified product using a NexteraXT tagmentation kit (Illumina). The library was sequenced over 500 cycles using a MiSeq sequencer. Reads were trimmed of sequencing adaptors using the Miseq reporter version 2.0.26. Low-quality sequences (defined as all sequence within each read following the first residue with a Phred score below 20) were removed from each read; quality control statistics and paired-end mapping of each read were performed using FastQC and custom bash scripts (De Wit et al. 2012). Nucleotide composition histograms and quality control boxplots are shown for each read in Supplementary Material Fig. S5. The resulting library was estimated to contain 61.9% duplicate reads, and 4.7% singletons. This library has been deposited in NCBI SRA (ID PRJNA518128).

To estimate read coverage against the *Amphidinium* plastid genome, a composite library consisting of all minicircle sequences previously reported from *A. carterae* CCMP1314/CCMP 1102/6, and the complete MMETSP transcriptome cDNA libraries of *A. carterae* CCMP1314 that had been cleaned of residual sequence contamination using a previously defined protocol (Dorrell et al. 2017; Marron et al. 2016) was assembled. To avoid duplication of plastid sequences within this library, the cDNA sequences corresponding to plastid-encoded proteins (Dorrell et al. 2017), as previously defined, were excluded from the MMETSP library. Each cleaned sequence paired-end read was searched against this library with BLASTn, and sequences that produced a top hit against a plastid minicircle sequence, over the complete length of the read sequence, and with a minimum threshold identity of 95%, were mapped to the minicircle sequence.

To assess the distribution of 5' end positions over minicircle sequences within the library, the paired-end read sequences were filtered for those that yielded a top hit against a minicircle sequence, and contained either a complete RNA adapter sequence, terminated at the 5' end with a region corresponding to the 3' terminal fragment of the RNA adapter, or terminated at the 3' end with a region corresponding to the complement of the 3' terminal fragment of the RNA adapter. The minimum length of RNA adapter used for this analysis corresponded to the last ten nt within the adapter sequence (TGGGTTGCAA), as this sequence was found (by BLASTn search) not to occur naturally in any of the screened minicircle sequence. Reads in which the RNA adapter was found in the reverse complement direction were reverse complemented, and each read was then trimmed at the 5' end to the end of the RNA adapter sequence. The trimmed reads were then searched again against the composite *Amphidinium* reference library. The position of the first residue (corresponding to the 5' ligation site of the transcript) and orientation (identifying sense/antisense transcription) of each trimmed read that mapped to an *Amphidinium* minicircle over the full length of the read, with at least 95% identity, was recorded.

RT-PCR experiments: cDNA synthesis reactions were performed using Superscript II reverse transcriptase (Sigma), and PCRs were performed with GoTaq DNA polymerase (Invitrogen), following the manufacturers' instructions. Oligo-d(A) primed RT-PCR, circular RT-PCR and RNA-ligase mediated 5'RACE were performed according to previously defined protocols (Barbrook et al. 2012; Dorrell et al. 2016b; Scotto-Lavino et al. 2006). PCR products were Sanger sequenced using an Applied Biosystems 3730xl DNA Analyser (Department of Biochemistry, University of Cambridge).

cDNA synthesis primers for sense transcripts were designed against the coding strands of minicircle sequence (Supplementary Material Table S2, section 2), and for antisense transcripts against the non-coding strands of minicircle sequence (Supplementary Material Table S2, sections 4, 5). Each cDNA synthesis primer was designed so that the final eight nt of the primer sequence was not found anywhere else, in any orientation, on any minicircle in the *A. carterae* plastid (Barbrook and Howe 2000; Barbrook et al. 2001; Hiller 2001; Nisbet et al. 2004), except in the desired annealing site, to minimise the possibility (for example) of mis-priming of primers designed for antisense transcripts to sense transcripts from the same minicircle.

To identify the full diversity of 5' and 3' termini associated with multi-copy and antisense transcripts by circular RT-PCR, five different PCR forward, and five different PCR reverse primers were designed against different regions of each minicircle sequence (Supplementary Material Table S2, sections 2, 5). For example, for the *psbA* minicircle, a PCR reverse primer was designed specific to the 5' end of the *psbA* gene, which would preferentially amplify multi-copy transcripts with mature 5' termini. Three further reverse primers were designed specific to non-coding regions of the *psbA* minicircle, upstream of the *psbA* mature transcript 5' terminus position that would prefer-

entially amplify multi-copy transcripts containing extensive UTR sequence. A final reverse primer was designed specific to the 3' end of *psbA* that would preferentially amplify transcripts with 5' termini located within the CDS. PCRs were then performed using each possible combination of forward and reverse primer, to amplify the ligated termini of transcripts covering minicircle core regions and antisense transcripts. Circular PCR was performed with the same thermal cycle scheme as in Barbrook et al. (2012): a 10 minute initial denaturation step at 95 °C, followed by 40 cycles consisting of 95 °C, 45 s; 55 °C, 45 s; and 72 °C, 2 minutes. Each circular RT-PCR was performed three times, using cDNA generated from independently isolated RNA samples, to maximise the capture of minicircle transcripts.

Northern blots: Probes for each northern blot were generated using a DIG Northern Starter kit (Roche). Probe template sequences were generated by fusion of selected minicircle amplicons to the T7 promoter region of pGEM-T Easy vector (Promega), following a previously established protocol (Dorrell et al. 2014; Nisbet et al. 2016). Probes were designed that were specific to the 5' and 3' UTRs of the *psbA* minicircle, as well as probes that were specific to the 5' and 3' ends of the *psbA* CDS (Supplementary Material Table S5). For the *petB/atpA* minicircle, probes were designed that were specific to the *petB* CDS, the 5' and 3' ends of the *atpA* CDS and the *petB* 5' UTR. To facilitate the direct comparison of sense and antisense transcripts, the RNA probes were complementary in sequence to the probes previously designed for sense transcripts from each minicircle, and identical RNA electrophoresis and detection conditions were used for sense and antisense transcript blots.

Northern blots, using freshly isolated RNA, were made and probed following previously established protocols (Dorrell et al. 2014, 2016a). Each Northern blot was made using 30 μg total cellular RNA, as this has been shown to be adequate to detect very low abundance and multi-copy transcripts in *H. triquetra* (Dang and Green 2010). Northern probes were hybridized using a DIG labelling kit (Roche), following the manufacturer's instructions. Chemiluminescence of DIG-conjugated horseradish peroxidase was detected in an Agilent Infinity 1260 over periods of between two minutes and twelve hours, dependent on the relative abundance of the corresponding transcript. Each northern blot experiment was performed twice using independently isolated RNA samples, and consistent banding patterns were identified in each case.

Acknowledgements

This work was supported by a UK Biotechnology and Biological Sciences Research Council doctoral training grant (B/F017464/1) to RGD and an MRC Confidence in Concept Grant to the University of Cambridge to RERN. RGD acknowledges additional funding via a Momentum Fellowship from the Centre National de la Recherche Scientifique (CNRS), and funding from the French Government 'Investissements d'Avenir' programmes MEMO LIFE (ANR-10-LABX-54) and PSL* Research University (ANR-1253 11-IDEX-0001-02. CJH acknowledges funding through the Gordon and Betty Moore Foundation through Grant GBMF4976.01, and by the UK Biotechnology and Biological Sciences Research Council (BBSRC) Synthetic Biology Research Centre 'OpenPlant' award (BB/L014130/1). The authors would like to thank Shilo Dickens and Davy Kurniawan (Department of Biochemistry, University of Cambridge) for assistance respectively with library preparation for next generation sequencing, and with northern blotting; and the Norfolk Federation of Womens' Institutes for the kind provision of their retiring room, during the preparation of this manuscript.

Appendix A. Supplementary Data

Supplementary data associated with this article can be found, in the online version, at https://doi.org/10.1016/j.protis.2019.06.001.

References

Bahl A, Davis PH, Behnke M, Dzierszinski F, Jagalur M, Chen F, Shanmugam D, White MW, Kulp D, Roos DS (2010) A novel multifunctional oligonucleotide microarray for *Toxoplasma gondii*. BMC Genomics **11**:603

Barbrook AC, Howe CJ (2000) Minicircular plastid DNA in the dinoflagellate *Amphidinium operculatum*. Mol Gen Genet **263**:152–158

Barbrook AC, Howe CJ, Nisbet RER (2018) Breaking up is hard to do: the complexity of the dinoflagellate chloroplast genome. Perspectives Phycol **0084**

Barbrook AC, Voolstra CR, Howe CJ (2014) The chloroplast genome of a *Symbiodinium* sp clade C3 isolate. Protist **165**:1–13

Barbrook AC, Howe CJ, Kurniawan DP, Tarr SJ (2010) Organization and expression of organellar genomes. Philos Trans R Soc Biol **365**:785–797

Barbrook AC, Santucci N, Plenderleith LJ, Hiller RG, Howe CJ (2006) Comparative analysis of dinoflagellate chloroplast genomes reveals rRNA and tRNA genes. BMC Genomics **7(297)**

Barbrook AC, Symington H, Nisbet RER, Larkum A, Howe CJ (2001) Organisation and expression of the plastid genome of the dinoflagellate *Amphidinium operculatum*. Mol Genet Genom **266**:632–638

Barbrook AC, Dorrell RG, Burrows J, Plenderleith LJ, Nisbet RER, Howe CJ (2012) Polyuridylylation and processing of transcripts from multiple gene minicircles in chloroplasts of the dinoflagellate *Amphidinium carterae*. Plant Mol Biol **79**:347–357

Barkan A (2011) Expression of plastid genes: organelle-specific elaborations on a prokaryotic scaffold. Plant Physiol **155**:1520–1532

Blankenberg D, Gordon A, Von Kuster G, Coraor N, Taylor J, Nekrutenko A, Team G (2010) Manipulation of FASTQ data with Galaxy. Bioinformatics **26**:1783–1785

Castandet B, Hotto AM, Fei Z, Stern DB (2013) Strand-specific RNA sequencing uncovers chloroplast ribonuclease functions. FEBS Lett **587**:3096–3101

Castandet B, Hotto AM, Strickler SR, Stern DB (2016) ChloroSeq, an optimized chloroplast RNA-seq bioinformatic pipeline, reveals remodeling of the organellar transcriptome under heat stress. G3 **6**:2817–2827

Dang Y, Green BR (2009) Substitutional editing of *Heterocapsa triquetra* chloroplast transcripts and a folding model for its divergent chloroplast 16S rRNA. Gene **442**:73–80

Dang Y, Green BR (2010) Long transcripts from dinoflagellate chloroplast minicircles suggest ŕolling circleť ranscription. J Biol Chem **285**:5196–5203

De Wit P, Pespeni MH, Ladner JT, Barshis DJ, Seneca F, Jaris H, Therkildsen NO, Morikawa M, Palumbi SR (2012) The simple fool's guide to population genomics via RNA-Seq: an introduction to high-throughput sequencing data analysis. Mol Ecol Resour **12**:1058–1067

Del Cortona A, Leliaert F, Bogaert KA, Turmel M, Boedeker C, Janouskovec J, Lopez-Bautista JM, Verbruggen H, Vandepoele K, De Clerck O (2017) The plastid genome In Cladophorales green algae is encoded by hairpin plasmids. Curr Biol **27**:3771–3782

Dorrell RG, Howe CJ (2012) Functional remodeling of RNA processing in replacement chloroplasts by pathways retained from their predecessors. Proc Natl Acad Sci USA **109**:18879–18884

Dorrell RG, Hinksman GA, Howe CJ (2016a) Diversity of transcripts and transcript processing forms in plastids of the dinoflagellate alga *Karenia mikimotoi*. Plant Mol Biol **90**:233–247

Dorrell RG, Drew J, Nisbet RER, Howe CJ (2014) Evolution of chloroplast transcript processing in *Plasmodium* and its chromerid algal relatives. PLoS Genet **10**, e1004008

Dorrell RG, Klinger CM, Newby RJ, Butterfield ER, Richardson E, Dacks JB, Howe CJ, Nisbet RER, Bowler C (2016b) Progressive and biased divergent evolution underpins the origin and diversification of peridinin dinoflagellate plastids. Mol Biol Evol **34**:361–379

Dorrell RG, Gile G, McCallum G, Méheust R, Bapteste EP, Klinger CM, Brillet-Guéguen L, Freeman KD, Richter DJ, Bowler C (2017) Chimeric origins of ochrophytes and haptophytes revealed through an ancient plastid proteome. eLife **6**:23717

Fujii H, Chiou TJ, Lin SI, Aung K, Zhu JK (2005) A miRNA involved in phosphate-starvation response in *Arabidopsis*. Curr Biol **15**:2038–2043

Gachon CMM, Heesch S, Kuepper FC, Achilles-Day UEM, Brennan D, Campbell CN, Clarke A, Dorrell RG, Field J, Gontarek S, et al. (2013) The CCAP KnowledgeBase: linking protistan and cyanobacterial biological resources with taxonomic and molecular data. Syst Biodiver **11**:407–413

Gavelis GS, White RA, Suttle CA, Keeling PJ, Leander BS (2015) Single-cell transcriptomics using spliced leader PCR: Evidence for multiple losses of photosynthesis in polykrikoid dinoflagellates. BMC Genomics **16**:528

Georg J, Honsel A, Voss B, Rennenberg H, Hess WR (2010) A long antisense RNA in plant chloroplasts. New Phytol **186**:615–622

Green BR (2011) Chloroplast genomes of photosynthetic eukaryotes. Plant J **66**:34–44

Griffith OM (1991) Cesium chloride gradients in carbon fiber fixed angle rotor for purification of viruses, organelles, and plasmid DNA. Am Biotechnol Lab **9**, 24, 26

Haxo FT, Kycia JH, Somers GF, Bennett A, Siegelman HW (1976) Peridinin chlorophyll A proteins of dinoflagellate *Amphidinium carterae* (Plymouth 450). Plant Physiol **57**:297–303

Hiller RG (2001) 'Empty' minicircles and petB/atpA and psbD/psbE (cytb559 alpha) genes in tandem in *Amphidinium carterae* plastid DNA. FEBS Lett **505**:449–452

Hotto AM, Germain A, Stern DB (2012) Plastid non-coding RNAs: emerging candidates for gene regulation. Trends Plant Sci **17**:737–744

Hotto AM, Castandet B, Gilet L, Higdon A, Condon C, Stern DB (2015) *Arabidopsis* chloroplast mini-ribonuclease III participates in rRNA maturation and intron recycling. Plant Cell **27**:724–740

Howe CJ, Nisbet RER, Barbrook AC (2008) The remarkable chloroplast genome of dinoflagellates. J Exp Bot **59**:1035–1045

Janouškovec J, Horák A, Oborník M, Lukeš J, Keeling PJ (2010) A common red algal origin of the apicomplexan, dinoflagellate, and heterokont plastids. Proc Natl Acad Sci USA **107**:10949–10954

Janouškovec J, Sobotka R, Lai DH, Flegontov P, Koník P, Komenda J, Ali S, Prásil O, Pain A, Oborník M, et al. (2013) Split photosystem protein, linear-mapping topology, and growth of structural complexity in the plastid genome of *Chromera velia*. Mol Biol Evol **30**:2447–2462

Klinger CM, Paoli L, Newby RJ, Wang MY, Carroll HD, Leblond JD, Howe CJ, Dacks JB, Bowler C, Cahoon AB, et al. (2018) Plastid transcript editing across dinoflagellate lineages shows lineage-specific application but conserved trends. Genome Biol Evol **10**:1019–1038

Lang BF, Burger G (2007) Purification of mitochondrial and plastid DNA. Nat Protoc **2**:652–660

Laslett D, Canback B (2004) ARAGORN, a program to detect tRNA genes and tmRNA genes in nucleotide sequences. Nucleic Acids Res **32**:11–16

Leung SK, Wong JTY (2009) The replication of plastid minicircles involves rolling circle intermediates. Nucleic Acids Res **37**:1991–2002

Lima-Mendez G, Faust K, Henry N, Decelle J, Colin S, Carcillo F, Chaffron S, Ignacio-Espinosa JC, Roux S, Vincent F, et al. (2015) Ocean plankton. Determinants of community structure in the global plankton interactome. Science **348**:1262073

Lin SJ, Zhang HA, Zhuang YY, Tran B, Gill J (2010) Spliced leader-based metatranscriptomic analyses lead to recognition of hidden genomic features in dinoflagellates. Proc Natl Acad Sci USA **107**:20033–20038

Lowe TM, Eddy SR (1997) tRNAscan-SE: A program for improved detection of transfer RNA genes in genomic sequence. Nucleic Acids Res **25**:955–964

Luro S, Germain A, Sharwood RE, Stern DB (2013) RNase J participates in a pentatricopeptide repeat protein-mediated 5' end maturation of chloroplast mRNAs. Nucleic Acids Res **41**:9141–9151

Marron AO, Ratcliffe S, Wheeler GL, Goldstein RE, King N, Not F, de Vargas C, Richter DJ (2016) The evolution of silicon transport in eukaryotes. Mol Biol Evol **33**:3226–3248

Mungpakdee S, Shinzato C, Takeuchi T, Kawashima T, Koyanagi R, Hisata K, Tanaka M, Goto H, Fujie M, Lin S, et al. (2014) Massive gene transfer and extensive RNA editing of a symbiotic dinoflagellate plastid genome. Genome Biol Evol **6**:1408–1422

Muñoz-Gómez SA, Mejía-Franco FG, Durnin K, Colp M, Grisdale CJ, Archibald JM, Slamovits CH (2017) The new red algal subphylum Proteorhodophytina comprises the largest and most divergent plastid genomes known. Curr Biol **27**:1677–1684

Nassoury N, Wang Y, Morse D (2005) Brefeldin a inhibits circadian remodeling of chloroplast structure in the dinoflagellate gonyaulax. Traffic **6**:548–561

Nelson MJ, Dang YK, Filek E, Zhang ZD, Yu VWC, Ishida K, Green BR (2007) Identification and transcription of transfer RNA genes in dinoflagellate plastid minicircles. Gene **392**:291–298

Nimmo I, Barbrook AC, Lassadi I, Chen JE, Geisler K, Smith AG, Aranda M, Purton S, Waller RF, Nisbet RER, Howe CJ (2019) Genetic transformation of the dinoflagellate chloroplast. eLife **8**:e45292

Nisbet RER, Koumandou VL, Barbrook AC, Howe CJ (2004) Novel plastid gene minicircles in the dinoflagellate *Amphidinium operculatum*. Gene **331**:141–147

Nisbet RER, Kurniawan DP, Bowers HD, Howe CJ (2016) Transcripts in the *Plasmodium* apicoplast undergo cleavage at tRNAs and editing, and include antisense sequences. Protist **167**:377–388

Nisbet RER, Hiller RG, Barry ER, Skene P, Barbrook AC, Howe CJ (2008) Transcript analysis of dinoflagellate plastid gene minicircles. Protist **159**:31–39

Okamoto OK, Hastings JW (2003) Novel dinoflagellate clock-related genes identified through microarray analysis. J Phycol **39**:519–526

Oldenburg DJ, Bendich AJ (2004) Most chloroplast DNA of maize seedlings in linear molecules with defined ends and branched forms. J Mol Biol **335**:953–970

Owari S, Hayashi A, K-i Ishida (2014) Subcellular localization of minicircle DNA in the dinoflagellate *Amphidinium massartii*. Phycol Res **62**:1–8

Richardson E, Dorrell RG, Howe CJ (2014) Genome-wide transcript profiling reveals the coevolution of chloroplast gene sequences and transcript processing pathways in the fucoxanthin dinoflagellate *Karlodinium veneficum*. Mol Biol Evol **31**:2376–2386

Rott R, Drager RG, Stern DB, Schuster G (1996) The 3' untranslated regions of chloroplast genes in *Chlamydomonas reinhardtii* do not serve as efficient transcriptional terminators. Mol Gen Genet **252**:676–683

Scotto-Lavino E, Du G, Frohman MA (2006) Amplification of 5' end cDNA with' new RACE'. Nature Protoc **1**:3056–3061

Sharwood RE, Halpert M, Luro S, Schuster G, Stern DB (2011) Chloroplast RNase J compensates for inefficient transcription termination by removal of antisense RNA. RNA **17**:2165–2176

Suggett DJ, Warner ME, Leggat W (2017) Symbiotic dinoflagellate functional diversity mediates coral survival under ecological crisis. Trends Ecol Evol **32**:735–745

Wang YL, Morse D (2006) Rampant polyuridylylation of plastid gene transcripts in the dinoflagellate *Lingulodinium*. Nucleic Acids Res **34**:613–619

Wang YL, Jensen L, Hojrup P, Morse D (2005) Synthesis and degradation of dinoflagellate plastid-encoded psbA proteins are light-regulated, not circadian-regulated. Proc Natl Acad Sci USA **102**:2844–2849

Wick RR, Judd LM, Gorrie CL, Holt KE (2017) Unicycler: Resolving bacterial genome assemblies from short and long sequencing reads. PLoS Comput Biol **13**:e1005595

Zandueta-Criado A, Bock R (2004) Surprising features of plastid *ndhD* transcripts: addition of non-encoded nucleotides and polysome association of mRNAs with an unedited start codon. Nucleic Acids Res **32**:542–550

Zauner S, Greilinger D, Laatsch T, Kowallik KV, Maier UG (2004) Substitutional editing of transcripts from genes of cyanobacterial origin in the dinoflagellate *Ceratium horridum*. FEBS Lett **577**:535–538

Zghidi-Abouzid O, Merendino L, Buhr F, Ghulam MM, Lerbs-Mache S (2011) Characterization of plastid *psbT* sense and antisense RNAs. Nucleic Acids Res **39**:5379–5387

Zhang Z, Green BR, Cavalier-Smith T (1999) Single gene circles in dinoflagellate chloroplast genomes. Nature **400**:155–159

Zhang ZD, Cavalier-Smith T, Green BR (2002) Evolution of dinoflagellate unigenic minicircles and the partially concerted divergence of their putative replicon origins. Mol Biol Evol **19**:489–500

Zhelyazkova P, Sharma CM, Förstner KU, Liere K, Vogel J, Börner T (2012) The primary transcriptome of barley chloroplasts: numerous noncoding RNAs and the dominating role of the plastid-encoded RNA polymerase. Plant Cell **24**:123–136